# Future prospects of fluoride based upconversion nanoparticles for emerging applications in biomedical and energy harvesting

S. P. Tiwari, S. K. Maurya, R. S. Yadav, A. Kumar, V. Kumar, Marie-France Joubert, H. C. Swart

JVST B
Journal of Vacuum Science & Technology B

# Future prospects of fluoride based upconversion nanoparticles for emerging applications in biomedical and energy harvesting

Cite as: J. Vac. Sci. Technol. B **36**, 060801 (2018); https://doi.org/10.1116/1.5044596
Submitted: 14 June 2018 . Accepted: 04 September 2018 . Published Online: 09 November 2018

**Surya P. Tiwari, Sachin K. Maurya, Ram S. Yadav, Abhishek Kumar, Vinod Kumar, Marie-France Joubert, and Hendrik C. Swart**

# Future prospects of fluoride based upconversion nanoparticles for emerging applications in biomedical and energy harvesting

Surya P. Tiwari,[1] Sachin K. Maurya,[2] Ram S. Yadav,[3,a)] Abhishek Kumar,[2] Vinod Kumar,[1,4,5] Marie-France Joubert,[6] and Hendrik C. Swart[1,b)]
[1]*Department of Physics, University of Free State, Bloemfontein 9300, South Africa*
[2]*Department of Applied Physics, Indian Institute of Technology (Indian School of Mines), Dhanbad 826004, India*
[3]*Department of Physics, Banaras Hindu University, Varanasi 221005, Uttar Pradesh, India*
[4]*Université Clermont Auvergne, CNRS, SIGMA Clermont, Institut de Chimie de Clermont-Ferrand (ICCF), 63000 Clermont-Ferrand, France*
[5]*Centre for Energy Studies, Indian Institute of Technology Delhi, New Delhi 110016, India*
[6]*Univ Lyon, Université Claude Bernard Lyon 1, CNRS, Institut Lumière Matière, F-69622 Villeurbanne, France*

(Received 14 June 2018; accepted 4 September 2018; published 9 November 2018)

Rare earth doped/codoped phosphors have been extensively studied for different types of applications based on their intense luminescence features. For this, researchers have tried to choose the inorganic host matrices having both a low phonon cut-off frequency and a high refractive index. Many articles have been published on oxide based phosphor materials, but due to their high cut-off phonon frequency, use of these materials is restricted for optical based applications. This is why additional research has been carried out on fluoride based host materials because of their low phonon frequencies, low composition degradation, and high quantum efficiency. In this paper, the authors review the rare earth fluoride based host nano- and micromaterials for different applications and discuss possible mechanisms.  https://doi.org/10.1116/1.5044596

## I. INTRODUCTION

Upconversion (UC) phosphor materials doped/codoped with rare earth elements have attracted the interest of researchers due to their multipurpose applications.[1–8] The biological application of UC materials is possible due to key material properties made possible by the fluoride based phosphor materials.[4,6] Thus, due to their high luminescence intensity, low phonon frequency, and high refractive index, fluoride based UC phosphor materials are preferred to oxide based host materials. Core-shell design as well as surface functionalization of nanophosphors was developed to engineer various medical probes for therapy purposes. Several review articles were recently published on this subject.[9–11] Furthermore, with the appropriate light irradiation photosensitizers, the absorbed optical energy is transferred to surrounding oxygen molecules, generating cytotoxic singlet oxygen or reactive oxygen species to kill cancer cells. Chen *et al.*[12] developed $NaGdF_4$:Yb:Er upconversion nanoparticle (UCNPs) to be used as part of a multifunctional platform. They coated these UCNPs with bovine serum albumin (BSA) and obtained UCNP@BSA nanoparticles in the process with great solubility and stability in physiological environments. They loaded two types of dye molecules, including a photosensitizer, Rose Bengal (RB), and a near infrared (NIR) absorbing dye, IR825, into the BSA layer of the UCNP@BSA nanoparticles. In the UCNP@BSA-RB&; IR825 system, the RB absorbs green light emitted from the UCNPs under 980 nm excitation to induce photodynamic cancer cell killing, while the IR825, whose absorbance shows no overlap with the UC excitation and emission wavelengths, offers nanoparticles strong photothermal performance under 808 nm laser irradiation. The obtained dual-dye loaded nanoparticles were able to kill cancer via combined photothermal and photodynamic therapies, both of which are induced by NIR light with high tissue penetration, in a synergistic manner both *in vitro* and *in vivo*. Additionally, the paramagnetic and optical properties of $Gd^{3+}$-doped UCNPs can further be used for *in vivo* dual modal imaging.[12] This type of research was reviewed by Kim *et al.*[13] Fluoride materials such as $NaYF_4$/$NaGdF_4$: $Er^{3+}$/$Yb^{3+}$ are very efficient materials, which exhibit green radiation after infrared excitation. In the $NaYF_4$ host, the site of $Y^{3+}$ is substituted by the rare earth dopant ions ($Er^{3+}$, $Ho^{3+}$, or $Yb^{3+}$). The UC emission of such a fluoride phosphor material has been reported by *Kano et al.*[14] They determined the UC efficiency of this phosphor material with different doping concentrations of $Er^{3+}$/$Yb^{3+}$. The optimized emission intensity was recorded for $Er^{3+}$/$Yb^{3+}$ codoped $SrWO_4$ phosphor by Pandey *et al.*[15] have also shown the UC emission efficiency of a variety of phosphor samples by codoping with Yb, Er, Yb, and Tm. They used a model to show the efficiency and the UC mechanism evolved in phosphor material. It was also reported that the UC efficiency was reduced by several orders of magnitude after incorporation of impurity phases. A detailed study

Note: This paper is part of the Special Topic Collection Honoring Paul Holloway for Contributions in Luminescent Materials Growth, Synthesis and Characterization.
a)Electronic mail: ramsagaryadav@gmail.com
b)Electronic mail: swarthc@ufs.ac.za

on the efficiency of this phosphor material has been reported by Thoma *et al.*,[16] in which they described the phase diagram of NaF-Y, Nd, Lu, or Gd. At high temperatures, they found irreversible melting of the hexagonal phases, which is responsible for the change of the hexagonal phase of the sample to a cubic phase at high temperatures. The structural characterization of the hexagonal form of $NaNdF_4$ has also been reported by Burns *et al.*[17] In addition to $NaNdF_4$, other fluoride hosts such as $NaGdF_4$ and $NaEuF_4$ have also been reported by different research groups[18,19] including their method of synthesis and enhanced UC emission intensity.

The UC mechanism is a very interesting branch of optics in which large numbers of photons are emitted after excitation with lower energy photons. The mechanisms of UC phenomena have been studied by numerous research groups since its discovery in 1959.[20,21]

## II. UC MECHANISM OF RARE EARTH DOPED PHOSPHORS

There are many reviews and research articles related to upconverting materials and to the different mechanisms leading to UC and Auzel's review of 2004 was the first extensive review in which UC luminescence microscopy for biological applications is mentioned.[22] In this section, we briefly describe UC mechanisms and describe the fundamental differences between them and the two-photon excitation (TPE) as well as the second-harmonic generation (SHG) nonlinear processes.

There are many multiphoton processes, which generate photons whose energy exceeds that of the irradiation photons. Figure 1 shows a schematic diagram differentiating three basic processes: the SHG, simultaneous two-photon absorption (TPA), also called TPE when the exited state gives rise to radiative emission of a photon, and UC processes in which intermediate metastable levels of active ions have a determinant role. SHG is a second order nonlinear optical process which requires phase matching and symmetry restrictions. The output photon wavelength is accurately half of the input photon wavelength. SHG is commonly used for coherent generation of visible light and one of the most known nonlinear optical materials for such an application is $KH_2PO_4$. In a rare earth doped luminescent material, population of a real excited state of the active ion via the simultaneous absorption of two photons is a third order nonlinear process, which is a result of third order optical susceptibility of the material. For biological applications, TPE microscopy

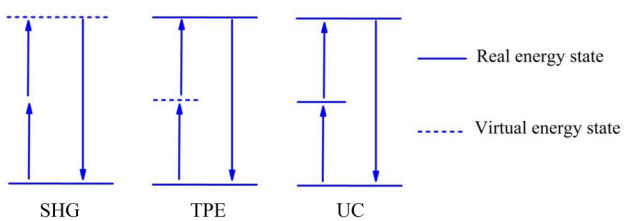


FIG. 1. Schematic diagram of the SHG, TPE, and UC luminescence.

is an alternative to confocal microscopy with clear advantages, for example, due to better transparency of tissues in the IR compared to visible light, high-resolution imaging in intact thick animal or human organs. More details about the SHG and TPE microscopy can be read in the references.[23,24] While TPE needs simultaneous absorption of two photons without an intermediate state and has a Femto second lifetime, the UC processes involve sequential absorption of two (or more) photons using real intermediate metastable states. The efficiency of these processes is thus higher compared to that of the TPE.

The UC phenomenon was first proposed and published by Bloembergen in 1959.[25] There are several important phenomena taking part in the UC processes, which are depicted in Fig. 2.[26–30] These include process of (a) ground state absorption and excited state absorption (ESA), (b) energy transfer upconversion (ETU), (c) a TPA, (d) cooperative sensitization upconversion (CSU), (e) cross relaxation (CR), and (f) photon avalanche (PA). Cooperative UC is an inefficient process, which is not included in the UC of nanoparticles at this stage. These processes are briefly discussed below.

### A. Excited state absorption

Since it occurs via sequential absorptions of the pump photons, this mechanism takes place in a multilevel ion system, which is the case for the $4f^n$ ground electronic configuration of rare earth ions that is illustrated in Fig. 2(a). It is a single ion process which can be efficient if there is an equal separation in the ladderlike structure (energy difference between $E_1$ and G equal to the energy difference between $E_2$ and $E_1$) and if $E_1$ is a metastable state for the reservoir capability. The ion is excited by a first pump photon from the ground state G level to the metastable state $E_1$ and then another pump photon promotes the ion from this intermediate state $E_1$ to a higher state $E_2$. Therefore, UC emission at shorter wavelength than the one of the excitation source will take place from the higher lying state $E_2$ to the ground state G. For efficient ESA, the ladderlike system of energy states of the active ions is necessary. It is well known that trivalent rare earth ions embedded into low-energy phonon materials, which is the case for fluoride materials, have such a ladder type of energy levels with metastable states.[22] Due to the single ion characteristic of ESA, the efficiency of this process is dependent on the dopant concentration.

### B. Energy transfer UC

Unlike the ESA process, which involves only one ion, a nonradiative energy transfer between two ions exists and plays a key role for ETU, as illustrated in Fig. 2(b). In the case of ETU due to successive energy transfers, the ion 1 is excited by a first pump photon absorption from the ground state G to the metastable state $E_1$. Then, due to the interaction between ion 1 (called sensitizer or donor) and ion 2 (called activator or acceptor), the energy accumulated by the sensitizer is transferred to the activator, which is thus excited in its E1 state. Further excitation of ion 1 into its $E_1$ state

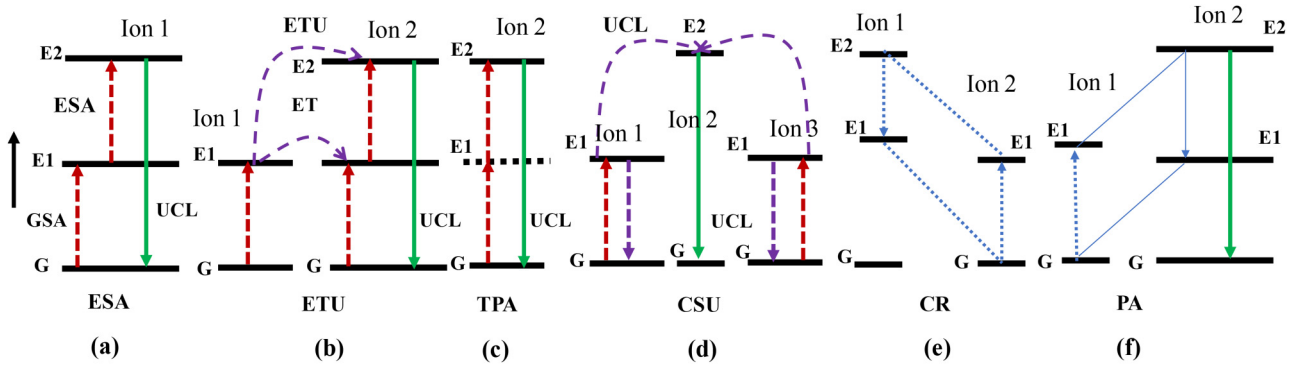


FIG. 2. UC mechanisms of rare earth doped/codoped particles: (a) ESA, (b) ETU, (c) TPA, (d) CSU, (e) CR, and (f) PA. The upward dotted arrows (photon excitation), and downward solid arrows (emission processes) lines are used for clarification. Reprinted with permission from Chen *et al.*, Chem. Rev. **114**(10), 5161 (2014). Copyright 2014 American Chemical Society.

may lead to energy transfer where both ions 1 and 2 are initially in their excited state $E_1$ promoting the acceptor (ion 2) in the higher lying state $E_2$ and the sensitizer (ion 1) in the ground state. UC emission will then take place from the higher lying state $E_2$ to the ground state G of the activator. In the case of ETU due to a cross relaxation energy transfer, each of the two neighboring ions 1 and 2 is promoted to the $E_1$ excited state via absorption of pump photons, and then energy transfer promotes the acceptor (ion 2) in the higher lying state $E_2$ and the sensitizer (ion 1) in the ground state. There are two different kinds of nonradiative energy. In one case, the energy difference between G and $E_1$ is equal to the energy difference between $E_1$ and $E_2$ states: it is a resonant energy transfer. If an energy mismatch exists between these two transitions, the energy transfer would be phonon assisted. The distance between sensitizer and activator plays an important role and needs to be considered in the efficiency of the ETU process, which may easily be calculated by using the concentration of the dopant.

The ETU process is the most essential part for the UC as it utilizes the ion pairs as sensitizer and activator. It is considered that $Eu^{3+}/Yb^{3+}$, $Tm^{3+}/Yb^{3+}$, $Er^{3+}/Yb^{3+}$, and $Ho^{3+}/Yb^{3+}$, which act as sensitizer and activator pairs, are the most frequently[31–34] used ones for the enhanced UC emission intensity. The sensitizer $Yb^{3+}$ ion has a large absorption cross section as compared to others. For fluoride nanoparticles, the optimized concentration of the $Yb^{3+}$ ion can be kept from 10% to 100% without evoking cross relaxations, because $Yb^{3+}$ has only two energy levels in its electronic structure. $Yb^{3+}$ ion may be excited by using pump photons in the wavelength range 975/980 nm depending on the host material.

### C. Cooperative sensitization UC

This process involves a 3 ion system in which ion 1 and ion 3 [Fig. 2(d)] are similar. Both are excited through absorption of pump photons. Then, as ion 1 and ion 3 act together in the elementary process of sensitization of ion 2 (energy transfer to ion 2), the process is qualified as cooperative: the energy accumulated by these two ions is given in one transfer to the activator (ion 2), which reaches a higher excited state. UC emission will then take place from this higher lying state to the ground state G of the activator. The CSU's efficiency is normally much lower than that of both ETU and ESA.[22] The CSU mechanisms have been published in detail and may be found in Refs. 3, 26, and 35–37.

### D. Cross relaxation

Cross relaxation is an energy transfer phenomena with an ion to ion interaction as shown in Fig. 2(e). In this interaction, ion 1 transfers the excited energy to ion 2 via (Ion 2) G + (Ion 1) $E_2 \rightarrow$ (Ion 2) $E_1$ + (Ion 1) $E_1$. In this process, ion 2 and ion 1 may be similar or dissimilar, and ion 2 can be in the excited state as well. The efficiency of the CR process is very closely connected to the dopant concentration. The CR process is one of the reasons for the concentration quenching mechanism, which is intentionally used for tuning the output color UC and also to construct a photon avalanche process.[35–37]

### E. Photon avalanche

Photon avalanche is the most complex among all UC processes. It is illustrated in Fig. 2(f). This process leads to UC emission when an excitation pump power above a certain threshold is used. A much less intense UC fluorescence is obtained below this threshold value, while above the pump threshold, the UC luminescence intensity increases by orders of magnitude. In this process, the pump photon is not resonant with transition from the ground state G of ions 1 or 2; it is only resonant with the transition $E_1 \rightarrow E_2$ of the UC emitting ion 2. If one ion 2 is promoted to its metastable state $E_1$, regardless of the mechanism of population of this state, and the pump photons are in resonant with the transition $E_1 \rightarrow E_2$, it may be further excited, via ESA, to its $E_2$ state. So, if the CR energy transfer schematized in Fig. 2(e) is efficient, this ion as well as one of its neighbor ions will be promoted in the metastable state $E_1$. Two ions are now available for $E_1 \rightarrow E_2$ ESA. Then, by the same feeding process, four ions will be further in state $E_1$ and so on. If the energy self-storage in state $E_1$ is efficient enough compared to energy losses of this level, the avalanche effect will start as soon as

the pump threshold is reached. The long time transient fluorescence at threshold is the clear signature of the photon avalanche process.

## III. FLUORIDE BASED HOST

The UC luminescence mechanism has usually been studied in different host matrices, such as halides (iodides, bromides, and chlorides), fluorides, oxides, vanadates, phosphates, and oxysulfides. Ideally, host matrices should be nonhygroscopic for good stability in air and in water and they should have low phonon frequencies, which minimize the losses due to nonradiative relaxation pathways. Halides such as iodides, bromides, and chlorides contain low phonon frequencies ($\leq 300\,cm^{-1}$) but are hygroscopic and have limited use. The oxides' host matrices have relatively large phonon frequencies (larger than $500\,cm^{-1}$) and good chemical stability. In comparison to other host matrices, fluorides have quite low phonon frequency (between 300 and $500\,cm^{-1}$), fine chemical stability of samples, and are easily dispersed in a colloidal state with water as well as several nonpolar solvents such as hexane, ethanol, chloroform, toluene, and dimethyl sulfoxide. So, fluoride host materials, mainly alkaline rare earth tetrafluoride ($AREF_4$), are the most popular hosts for UC emission.[33–38] Ledoux *et al.*[38] have recently given quite a complete overview of fluoride host characteristics and advantages for efficient UC luminescence.

## IV. SYNTHESIS

The synthesis of UC phosphor is the major challenge to the production of monodispersed NPs. These NPs exhibit a narrow size distribution and are highly soluble in an aqueous solution for the purpose of biological applications. The nucleation and growth process of the NPs are dependent on the crystallization method. The related nucleation growth process has been investigated by Victor Lamer; consequently, it is known as the LaMer mechanism.[39,40] The thermodynamic and kinetic description of the fundamental particle growth has been published in reference.[41] This research shows that NPs are mostly in the composition of the host lattice and agglomerated according to this parameter.

Among the existing kinds of UC host materials, fluorides have been established to be an ideal host for UC emissions with a high quantum yield due to the low phonon frequency and very high stability. To date, the $NaYF_4$ doped with $Yb^{3+}/Er^{3+}$, $Yb^{3+}/Ho^{3+}$, and $Yb^{3+}/Tm^{3+}$ are the most efficient UC materials to produce blue, green, and red emission.[42,43] Recently, many research groups have focused on the preparation methods/techniques, surface modification, and application of UCNPs in biological fields.[41–43] There are many methods to synthesize NPs; however, basically three methods are very common for fluoride based UCNPs synthesis and they are described as coprecipitation, hydrothermal and thermal decomposition methods.[44–64] Others synthetic strategies such as microemulsion synthesis, microwave-assisted synthesis, and ionic liquid synthesis have been also discussed recently.[42]

### A. Coprecipitation method

The coprecipitation method is the easiest method as compared to other approaches because of their favorable reaction conditions, low expense for required equipment, effortless protocols, and slow reaction times. Yi *at el.*[44] was the first to report on the coprecipitation synthesis method for synthesizing $NaYF_4:Yb^{3+}/Er^{3+}$ phosphor NPs, using ethylenediaminetetraacetic acid (EDTA), Fig. 3. In this method, particle size is controlled by varying the relative molar amount of the EDTA.

With the preparation of rare earth doped/codoped $NaYF_4$ phosphors by the coprecipitation method, annealing treatment is usually required to enhance the UC luminescence intensity that in turn allows the nanoparticles to aggregate and grow larger. Additionally, the capping reagents such as EDTA can become carbonized during annealing. This reduces the hydrophilicity of NPs. Moreover, by using a silica coating on the surface of the sample, the hydrophilic nature of the material may be enhanced, and it leads to an increase in the size of the NP. Therefore, the $NaYF_4$ phosphor synthesized by the coprecipitation technique has a limited application in the biomedical sciences.[45]

### B. Hydrothermal method

The hydrothermal technique is a chemical synthesis process carried out in a sealed atmosphere at high temperature and pressure. In a typical hydrothermal synthesis process specific reaction vessels, Teflon lined autoclaves are used for the sealed atmosphere reaction. It is an efficient and suitable process for preparing UCNPs and produces diverse controllable architectures and morphologies. For illustration, a variety of shapes of $NaYF_4$ crystals such as rod, prism, tube, disk, and octadecahedral shapes have been obtained by using this preparation technique.[46–48] Shang *et al.* synthesized different shapes of rare earth fluoride micro/nanocrystals.[49] They reported that different molar ratios of oleic acid

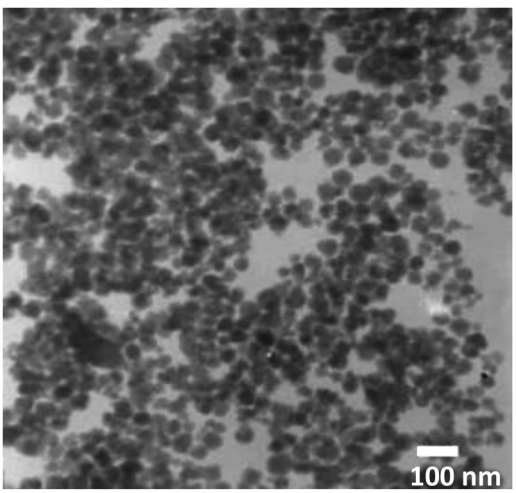


FIG. 3. TEM image of the pristine $NaYF_4:Yb^{3+}/Er^{3+}$ nanoparticles. The scale bar is 100 nm as indicated. Reprinted with permission from Yi *et al.*, Nano Lett. **4**, 2191 (2004). Copyright 2004 American Chemical Society.

(OA)/ligand ($Ln^{3+}$) and $F^{-}/Ln^{3+}$ have effects on the shapes of the crystals with changes from nanorods to hexagonals.

The advantages of adopting the hydrothermal route for synthesizing high quality UCNPs are (a) the use of simple equipment and the overall process is also simple (b) at a relatively low reaction temperature (commonly around 200 °C), (c) easy control of the structure, size, and morphology of the NPs, and (d) a high degree of purity yield. However, generally, the hydrophilicity of the UCNPs synthesized using the hydrothermal technique has not been high enough due to the presence of hydrophobic organic ligands (e.g., OA) on the surface of the nanoparticles.

Kumar *et al.* have synthesized different shapes of rare earth doped fluoride micro/nanocrystals ($YF_3$:$Tm^{3+}$/$Yb^{3+}$/$Ca^{2+}$).[50] They have reported on the doping effect of $Ca^{2+}$ on the $YF_3$:$Tm^{3+}$/$Yb^{3+}$ phosphor material. After increasing the concentration of the $Ca^{2+}$ ions, the shape and size of the fluoride based host phosphor particles were transformed from a dumbbell to a pyramid shape (Fig. 4). In a typical preparation method, $Y_2O_3$, $Tm_2O_3$, $Yb_2O_3$, and $CaCO_3$ were used as precursor materials. Concentrated HCl was added to these weighed materials and heated up to 80 °C. After a while, 20 ml of oleic acid along with 8 ml of ethanol was added to this solution and stirred for 15 min. Finally, to this solution $NH_4F$ was added as an aqueous solution and stirred for another 30 min. This solution was kept in a Teflon lined autoclave and heated at 190 °C for 24 h. After cooling down, the solution was washed with ethanol three times in order to remove the organic impurities. The obtained raw material was dried over night for further characterization and measurements.

In Fig. 4, the images collected by field emission scanning electron microscopy (FESEM) were shown for different concentrations of $Ca^{2+}$ ions (0, 10, 20, and 30 mol. %). The bitter gourdlike structures were found for 0 mol. % $Ca^{2+}$ ions [Fig. 4(a)]. After increasing the doping concentration of the $Ca^{2+}$ ions (10, 20, and 30 mol. %), well defined octahedral shaped particles were seen in the FESEM images [Figs. 4(b)–4(d)]. As the doping concentration was increased, the particle size decreased [Figs. 4(c) and 4(d)]. The optimized particle size was obtained for the sample ($YF_3$:$Tm^{3+}$/$Yb^{3+}$) doped with 10 mol. % of $Ca^{2+}$ ions.

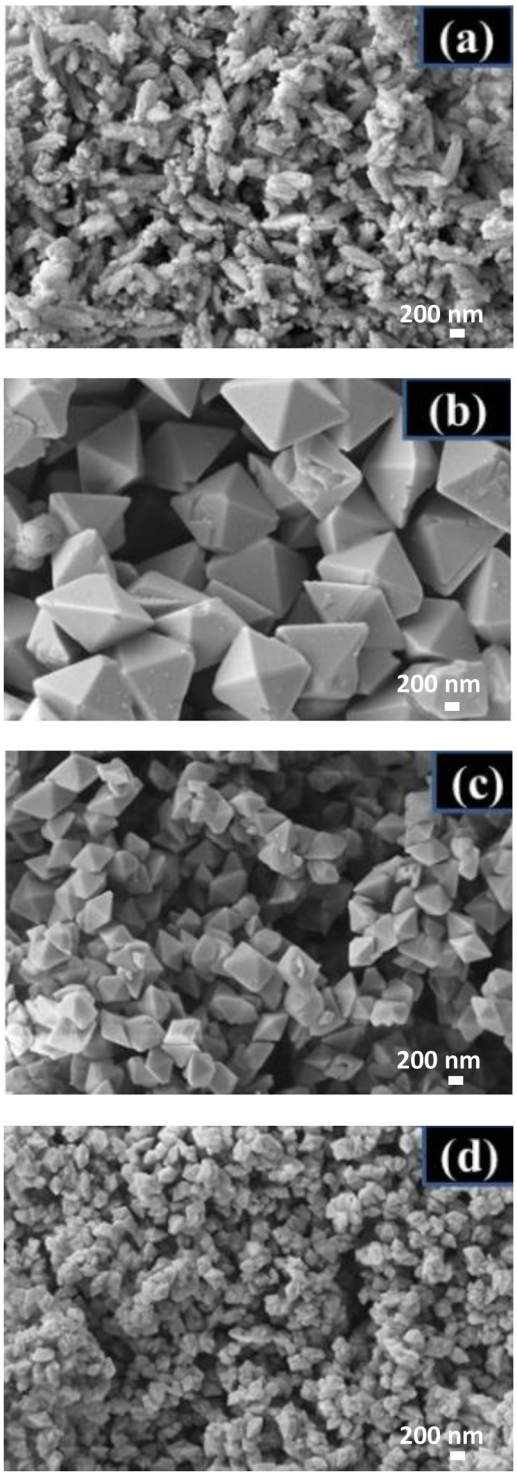


FIG. 4. FESEM images of $YF_3$:$Tm^{3+}$/$Yb^{3+}$ phosphor with different concentrations of $Ca^{2+}$ ions: (a) 0 mol. % (b) 10 mol. % (c) 20 mol. %, and (d) 30 mol. %. The scale bars of images are 200 nm. Reprinted with permission from Kumar *et al.*, Sensors Actuat. A: Physical **280**, 179–187 (2018). Copyright 2018 Elsevier.

### C. Thermal decomposition methods

In this method, the metal trifluoroacetate precursor is thermally decomposed to provide the desired metal fluorides. The thermal decomposition synthesis route is one of the most generally used strategies for the synthesis of UCNPs and has been implemented in the production of $AREF_4$ UCNPs such as $LiYF_4$,[51] $NaYF_4$,[52,53] $NaGdF_4$,[54,55] $NaLuF_4$,[56] and $KGdF_4$.[57] This method has also been utilized to produce lanthanide-doped fluorescent NPs, which is based on other host matrix, such as $GdF_3$[58] and $CaF_2$.[59] The thermal decomposition method also provides the best control of particle size and structure with a comparatively short reaction time and also produces a high quality yield with monodispersed materials.[60] The technique makes use of thermolysis of organometallic precursors, generally lanthanum trifluoroacetates/metal. Commercially obtainable Lanthanum trifluoroacetates precursors are generally prepared by reacting Lanthanum oxides with trifluoroacetic acid.[61] Normally, an elevated temperature (boiling) solvent

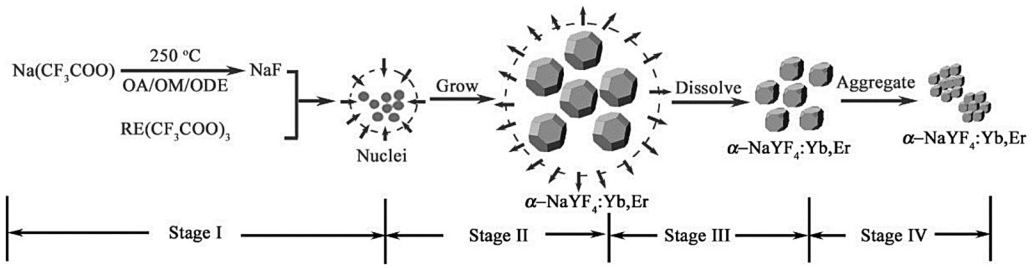


FIG. 5. Schematic diagram of the growth phases of α-$NaYF_4$:$Yb^{3+}$, $Er^{3+}$. Reprinted with permission from Mai *et al.*, J. Phys. Chem. C **111**, 13730 (2007). Copyright 2007 American Chemical Society.

such as 1-octadecene (ODE) solution of surface ligands is heated to slightly above the decomposition temperature of the precursors (over 300 °C). The solution of the requisite metal or lanthanum trifluoroacetates is introduced into the heated ligand solution for the reaction. Moreover, the reactants are quickly released due to the fast nucleation process.[62] With the aid of surface ligands such as oleylamine (OM) or OA, the particle size of the synthesized samples is controlled.[60] These ligands include polar top groups which coordinate to the growing particle throughout the reaction, along with extensive hydrocarbon tails which extend out to the bulk solution to give the requisite solubility.[60,63] In addition, the enhancement of the particle size is controlled by using surface ligands. The repulsive interaction technique is used for the optimization of the surface ligands to stop the agglomeration of the particles. The use of air susceptible metal precursors is required resulting in the need to frequently purge the system with an inert gas, as well as due to the toxic mutable products that are produce by the reaction.[64] The sample is collected following precipitation by centrifugation and then mixed with organic polar solvents and colloidally monodispersed precursors, which allows the sample to be kept for prolonged periods of time.[61] Yuan *et al.*[65] have also reported core cell modified structure by varying the concentration of silica/silver to get the improved upconversion emission. Figure 5 depicts the synthesis steps of cubic $NaYF_4$:$Yb^{3+}$/$Er^{3+}$ UCNPs, and by changing the concentration of reagents, reaction time, and reaction temperature, various shapes and sizes of $NaYF_4$:$Yb^{3+}$/$Er^{3+}$ UCNPs can be obtained.[64]

A modified preparation method has also been available, which takes advantage of the exceptional solubility properties of polyethylene glycol (PEG). In this modified method, polyethylenimine capping ligands were used, instead of the predictable OM or OA capping ligands, which are easily dispersed in aqueous media. In Figure 6, the shapes and sizes of synthesized UC phosphors are shown with respect to different annealing time intervals.[66]

In general, the thermal decomposition technique is used for the preparation of the hexagonal phase that is lanthanum doped (such as beta-$NaYF_4$) UCNPs with the particles diameter size ranging in the order of 15–40 nm. This method requires well controlled reaction temperatures, organic solvents, and moderate air sensitive precursors along with an inert atmosphere. The reproducibility of

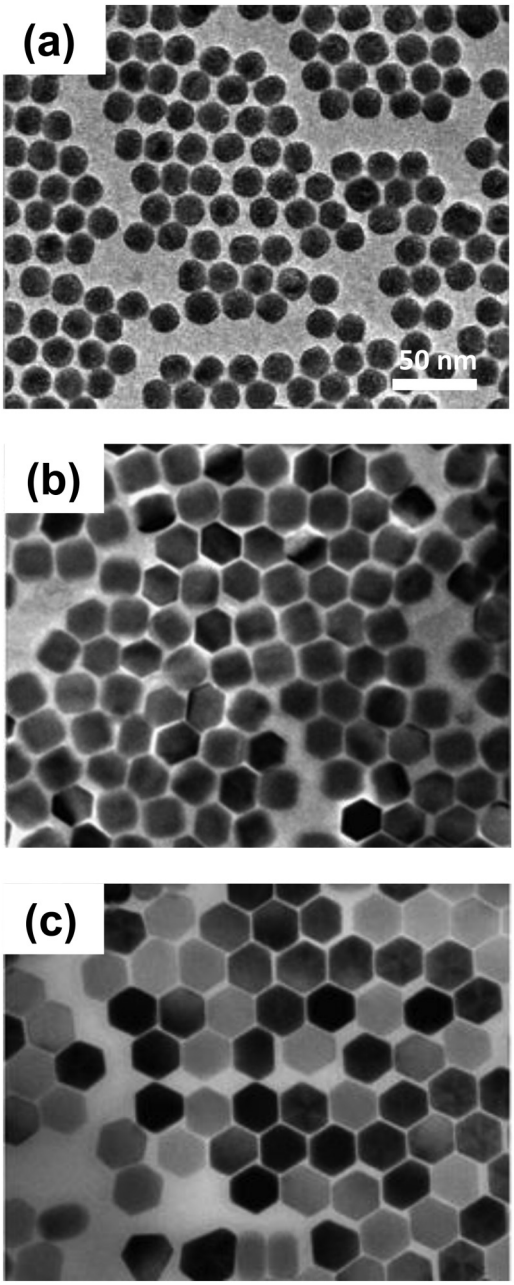


FIG. 6. TEM images of the $NaYF_4$ product [annealed at 330 °C, OA/ODE (1:1)] (a) for 15 min, (b) for 25 min, and (c) for 45 min. The precursors used were around 1.9 mmol $Na(CF_3COO)$ and 1 mmol $(Y(CF_3COO)_3$. Reprinted with permission from Mai *et al.*, J. Am. Chem. Soc. **19**, 6426 (2006). Copyright 2006 American Chemical Society.

UCNPs is a practical challenge in the temperature range of thermal decomposition. For colloidal stability, nonpolar capping ligands are required as well as surface modification for biological applications.[67]

## V. APPLICATIONS OF FLUORIDE BASED UC PHOSPHORS

The different RE phosphor based compounds are easily synthesized as discussed earlier and have numerous applications. These phosphors are nontoxic and biocompatible compounds. The RE doped phosphors give emissions from the UV to NIR range and therefore can be used in photonics, temperature sensing, chemotherapy, and biological imaging. The luminescence mechanisms of these materials are superior to those of conventional and endogenous fluorescent markers, which enable UC bioimaging as a matchless visualizing tool without any autofluorescence arising out of the biological tissues. The RE UC nanoparticles possess attractive structural, thermal, chemical, and optical features, such as narrow band width emission lines, long lifetimes, strong photostability, and thermal stability. Therefore, the research is concentrated on discovery and improving materials and their properties for especially UC bioimaging as biological luminescence marker applications.[66–87]

Among the different phosphors, the fluoride based RE doped phosphors are very attractive and have versatile utility in fields such as photonics, solar cells, temperature sensing, cancer therapy, chemotherapy, and biological imaging. The photonics and solar cell applications arise due to downconversion (DC) and quantum cutting (QC) processes.[88–93] For example, Guo *et al.* have synthesized $Ho^{3+}$, $Yb^{3+}$ codoped $BaGdF_5$ nanoparticles by the hydrothermal method and reported downshifting and quantum cutting emissions due to first and second order energy transfers. The emission of NIR photons observed at 980 and 1180 nm is due to cooperative downconversion and cross relaxation energy transfer processes. The theoretical quantum efficiency is estimated to be 192% for this material.[88] When the $Ho^{3+}$, $Yb^{3+}$ codoped $BaGdF_5$ nanoparticles are excited with 450 nm, the $Ho^{3+}$ ions are promoted to its $^5F_1$ state, which relax to the $^5F_3$ state nonradiatively. Due to cooperative energy transfer (CET) and CR processes, it gives Stoke emissions in the visible and NIR regions centered at 980 and 1180 nm due to the $Ho^{3+}$ and $Yb^{3+}$ ions. The QC process due to $Ho^{3+}$ ions in the NIR region is verified by time resolved spectroscopy. The NIR emissions at 980 and 1180 nm are due to the $^2F_{5/2} \rightarrow {}^2F_{7/2}$ manifolds of $Yb^{3+}$ ions and the $^5I_6 \rightarrow {}^5I_8$ transition of the $Ho^{3+}$ ions, respectively. Thus, it has also been proposed that these nanoparticles open the door for designing ultraefficient photonic devices in low band gap solar cells and thermophotovoltaic energy conversion, etc.

Zhang *et al.* have synthesized $Y_{6(1-x)}O_5F_8$:$xYb^{3+}$, 1% $Ho^{3+}$ microarchitectures by the hydrothermal method and reported QC emissions along with UC emission due to CETs. The emission of NIR photons observed at 980 and 1180 nm is due to cooperative downconversion and cross relaxation energy transfer processes.[89] The schematic presentation of the energy levels of $Ho^{3+}$and $Yb^{3+}$ ions is shown in Fig. 7. When the $Ho^{3+}$, $Yb^{3+}$ ions are excited with 360 and

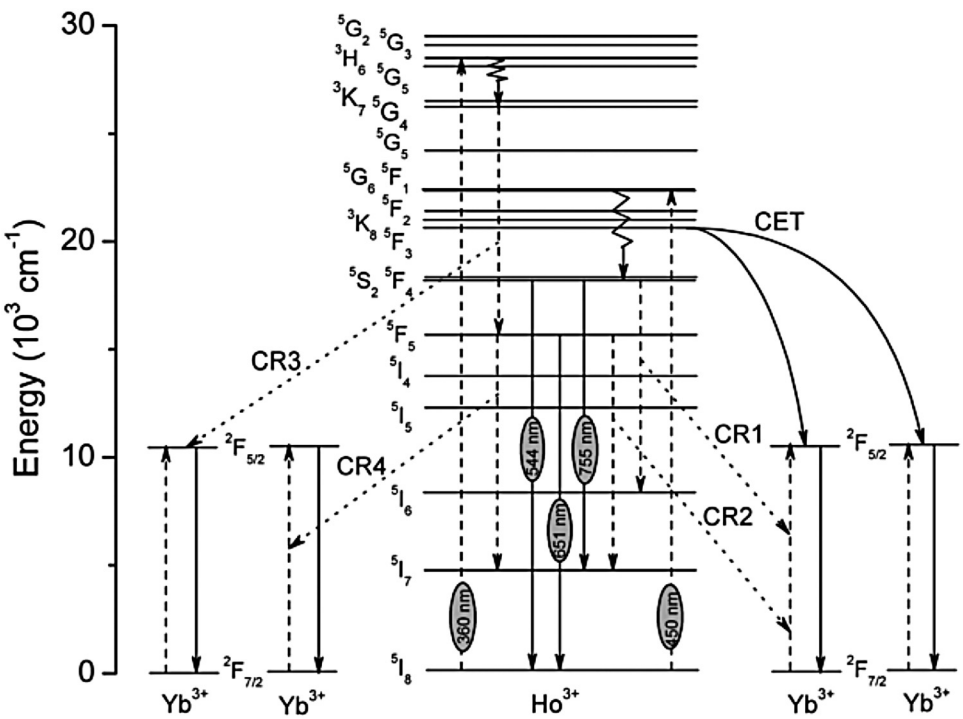


FIG. 7. Pathway of energy levels diagram of $Ho^{3+}$and $Yb^{3+}$ transitions using 360 and 450 nm excitation sources. Reproduced with permission from Zhang *et al.*, Dalton Trans. **42**, 3542 (2013). Copyright The Royal Society of Chemistry (RSC), see http://pubs.rsc.org/en/content/articlelanding/2013/dt/c2dt32463f#!divAbstract.

450 nm radiation, the $Ho^{3+}$ ions are promoted to the $^3H_6$ and $^5F_1$ states, which relax to the $^5G_4$ and $^5F_4$ states nonradiatively. Due to CET and CR processes, Stoke emissions are given in the visible and NIR regions centered at 980 and 1180 nm due to the $Ho^{3+}$ and $Yb^{3+}$ ions. The NIR emissions at 980 and 1180 nm are a result of the $^2F_{5/2} \rightarrow {}^2F_{7/2}$ transition ($Yb^{3+}$ ions) and the $^5I_6 \rightarrow {}^5I_8$ transition ($Ho^{3+}$ ions), respectively. They also emit visible photons upon 360 and 450 nm excitations.

The photoluminescence excitation (PLE) and PL spectra of different concentrations of $Yb^{3+}$ ions (0, 5, 10, and 15 mol. %) in $Y_6O_5F_8:Yb^{3+}/Ho^{3+}$ phosphor are shown in Fig. 8. The PLE spectrum, shown as an inset in Fig. 8(b), was measured by determining the emission at 980 nm, whereas the PL spectra were monitored upon excitation with 360 nm and 450 nm sources. The inset image in Fig. 8(a) shows that quantum cutting can be obtained by exciting the sample with 360 nm, and the same was obtained for an excitation of 450 nm.[89] The emission spectra show that the DC intensity of the visible regime decreases continuously on increasing the concentrations of the $Yb^{3+}$ ions, whereas that of NIR emission is an optimum at 10 mol. % [see Figs. 8(a) and 8(b)]. This occurs due to CET from $Ho^{3+}$ to $Yb^{3+}$ ions. This NIR emission may be used to increase the efficiency of the crystalline solar cells.

There is enormous interest in the spectral conversion for quantum cutting processes using three photons. In an interesting work, Yu *et al.* observed near infrared quantum cutting through a three step process (three photons) in $Tm^{3+}$ doped β-$NaYF_4$ nanophosphor.[93] The sample was excited using 470 nm, which promotes the ions from the ground state ($^3H_6$) to the excited state ($^1G_4$). When the sample is excited with a 470 nm source, the emission of three NIR photons occurs at 1165, 1466, and 1800 nm via three different emission processes. When the sample is further excited by a 798 nm source, the $Tm^{3+}$ ions are promoted to the $^3H_6$ state and give rise to the emission of two NIR photons at 1466 and 1800 nm along with another NIR photon at 808 nm. This excitation process increases the population of the ions in the $^3H_6$ state and enhances the intensity of these NIR photons. The three step emission processes are summarized to be (a) the first-step, $^1G_4 \rightarrow {}^3H_4$ at 1165 nm, (b) the second-step, $^3H_4 \rightarrow {}^3F_4$ at 1466 nm, and (c) the third-step, $^3F_4 \rightarrow {}^3H_6$ at 1800 nm. The photoluminescence emission spectra of the $Tm^{3+}$ ion have been observed on excitation with 470, 798, and 976 nm wavelengths.

Interestingly, in another set of experiments, the $Tm^{3+}/Yb^{3+}$ codoped phosphors also emits the NIR emission (Stoke emission) at 1800 nm from $Tm^{3+}$ ion on excitation with a 976 nm source. This is due to nonradiative energy transfer from $Yb^{3+}$ to $Tm^{3+}$ ions. The $Tm^{3+}/Yb^{3+}$ codoped sample was excited with a 976 nm diode laser, which promotes the $Yb^{3+}$ ions to its excited state ($^2F_{5/2}$) state from the ground state ($^2F_{7/2}$). These ions transfer their energy to the $Tm^{3+}$ ion in the $^3H_4$ state, which ultimately populates the $^3H_4$ state. As a result, the emission of NIR photon is possible at 1800 nm in the $Tm^{3+}/Yb^{3+}$ codoped sample, which matches the third-step emission process via the $^3F_4 \rightarrow {}^3H_6$ transition. The generation of these three photons, that is, 1165, 1466, and 1800 nm, through sequential depopulation of the ions from $^1G_4$ state leads to their applications not only in the field of low band gap solar cells but also thermovoltaic spectral conversion.[88,93]

Zhu *et al.* have prepared monodispersed $Pr^{3+}/Yb^{3+}$ codoped $NaGdF_4@NaYF_4$ active-core/inert-shell nanoparticles and studied the NIR quantum cutting luminescence in this material. In this case, the quantum cutting arises due to CET from $Pr^{3+}$ to $Yb^{3+}$ ions. They have introduced an extra $Yb^{3+}$ ion into the shell in order to prevent the adverse effect raised by concentration quenching. It forms an active-core/active-shell environment and improves the intensity of NIR emission. The schematic arrangement of the excitation and emission processes in the two cases is shown in Fig. 9.[94]

The $Pr^{3+}/Yb^{3+}$ codoped $NaGdF_4@NaYF_4$ active-core/inert-shell nanophosphors were excited by a 445 nm source and the spectra thus obtained are given in Fig. 10. The $Pr^{3+}$ ion gave an intense blue emission at 483 nm due to the $^3P_0 \rightarrow {}^3H_4$ transition. When codoped with $Yb^{3+}$ ions, the emission intensity at 483 nm decreased notably, whereas an intense NIR emission centered at 979 nm occurred due to the $^2F_{5/2} \rightarrow {}^2F_{7/2}$ transition ($Yb^{3+}$ ion). Since the $Yb^{3+}$ ions cannot be excited by 445 nm, therefore, the NIR emission occurred due to the CET process. Figure 10 also shows an increase in the intensity of the NIR band due to the addition of the $Yb^{3+}$ ion into the shell.

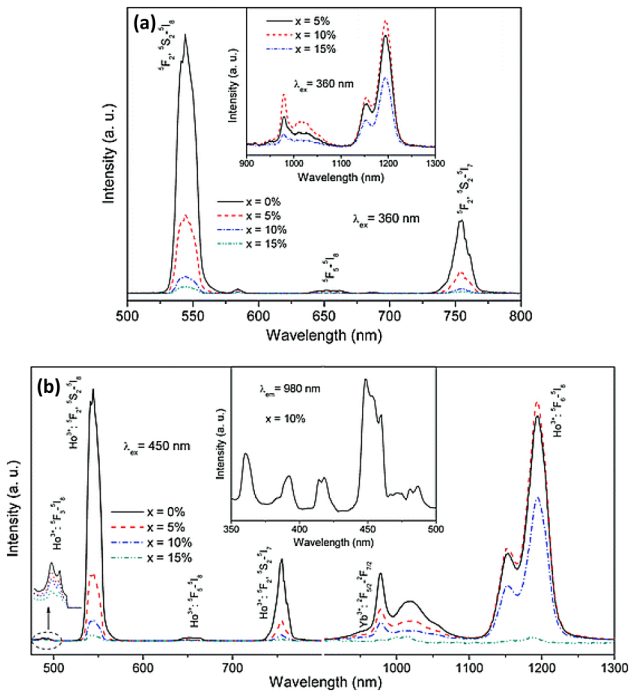


FIG. 8. Emission spectra of the $Y_6O_5F_8:Yb^{3+}/Ho^{3+}$ phosphor samples after exciting with 360 and 450 nm wavelengths. The inset in (a) shows the emission spectrum of $Y_6O_5F_8:Yb^{3+}/Ho^{3+}$ phosphor samples in the NIR region, whereas in (b) the excitation spectrum of $Y_6O_5F_8:Yb^{3+}/Ho^{3+}$ phosphor samples after exciting with a 980 nm laser source. Reproduced with permission from Zhang *et al.*, Dalton Trans. **42**, 3542 (2013). Copyright The Royal Society of Chemistry (RSC), see http://pubs.rsc.org/en/content/articlelanding/2013/dt/c2dt32463f#!divAbstract.

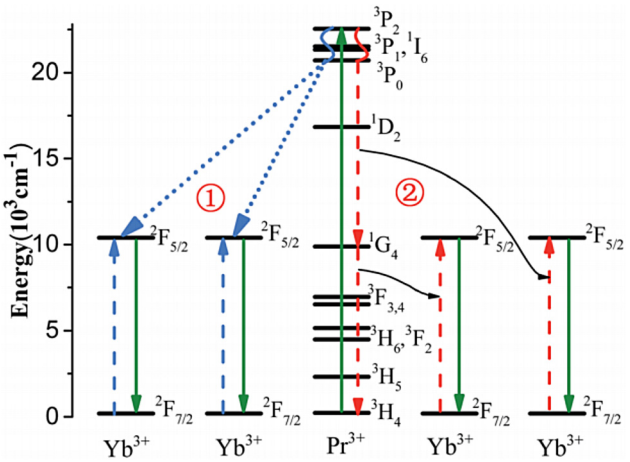


FIG. 9. Energy-level diagrams presenting the concept of quantum-cutting mechanisms in the $Pr^{3+}/Yb^{3+}$ couples. Reproduced with permission from Zhu *et al.*, Nanoscale **6**, 10500 (2014). Copyright The Royal Society of Chemistry (RSC), see http://pubs.rsc.org/en/content/articlelanding/2014/nr/c4nr02785j#!divAbstract.

Wang *et al.* have also reported quantum cutting in $Eu^{3+}$ doped $NaYbF_4$ nanotubes through cooperative DC energy transfer, and cross relaxation processes. The sample was excited by using a 393 nm source, which promotes the $Eu^{3+}$ ions from the $^7F_0$ to $^5L_6$ level. The ions in this state relax nonradiatively to populate different low lying states. As a result, a large number of radiative transitions took place at 465, 488, 510, 555, 591, 615, 650, and 695 nm wavelengths. Some of the $Eu^{3+}$ ions present in the $^5D_2$ state transfer their energy to $^2F_{7/2}$ state of the two $Yb^{3+}$ ions cooperatively. This leads to a quantum cutting process by the broad emission of two NIR photons in the 977–1015 nm region. The cross relaxations between $Eu^{3+}$ and $Yb^{3+}$ ions also promote the ions in the upper states of the two ions, which improves the emission intensity of the NIR transition.[95] The schematic representation of CET and cross relaxation of the ions is shown in Fig. 11.

The emissions of visible and NIR photons as a function of different $Eu^{3+}$ concentrations are shown in Fig. 12. It is clear from the figure that the emission intensity increased with increasing concentration up to a certain level and then decreased considerably due to concentration quenching. The emission intensity was an optimum at 3 mol. % concentration of the $Eu^{3+}$ ion for the visible and NIR photons, respectively. The reduction in the emission intensity was found to be due to shorter distances than the critical distance between the $Eu^{3+}/Yb^{3+}$ ions, respectively. Thus, the $Eu^{3+}$ doped $NaYbF_4$ nanotubes gave efficient quantum cutting emissions and can be used in photonic devices and solar cells.[95]

On the other hand, the fluoride based RE doped nanophosphors show interesting frequency UC in which low-energy NIR photons are converted into high energy UV/visible photons. The RE doped fluoride nanophosphors give rise to anti-Stokes emissions in the visible and NIR regions, which are used in optical devices, temperature sensing, chemotherapy, photothermal treatment, biomarkers, biological

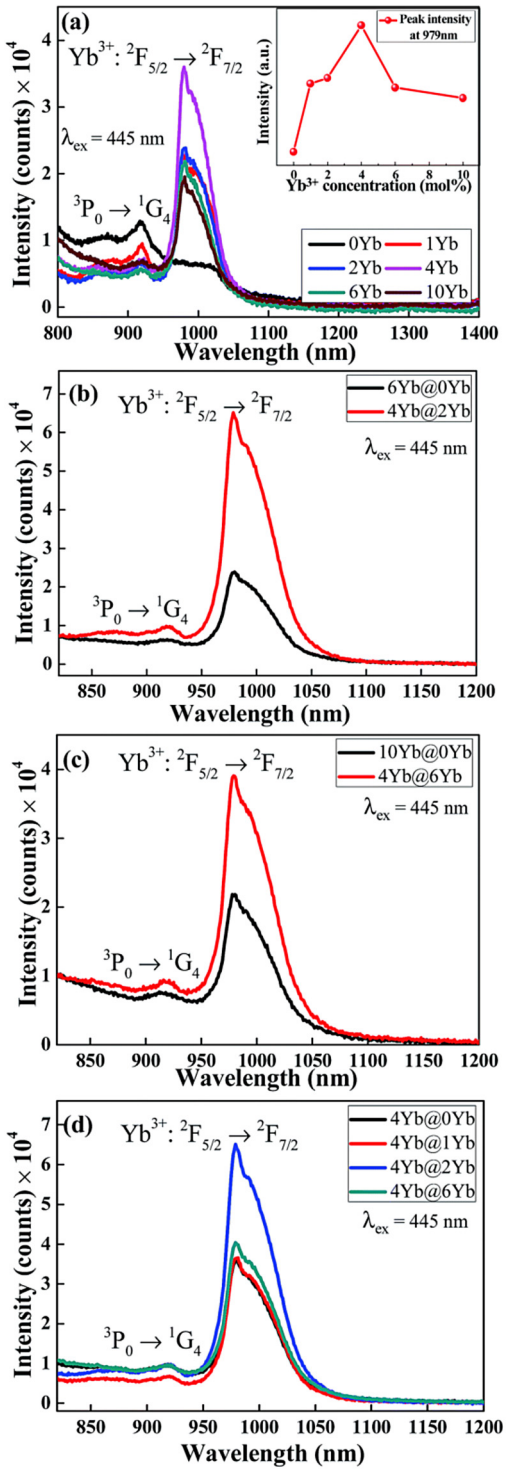


FIG. 10. (a) NIR PL spectra of the $Pr^{3+}/Yb^{3+}$ codoped $NaGdF_4@NaYF_4$ samples with various $Yb^{3+}$ concentrations. The inset shows the luminescence intensity with $Yb^{3+}$ concentrations ($Pr^{3+}$ = 0.1 mol. %, $Yb^{3+}$ = 0, 1, 2, and 6 mol. %). (b) Comparison of NIR luminescence spectra for the $Pr^{3+}/Yb^{3+}$ codoped $NaGdF_4@Yb^{3+}$:$NaYF_4$ ($Pr^{3+}$ = 0.1 mol. %, $Yb^{3+}$ = 4 mol. %) and $Pr^{3+}/Yb^{3+}$ codoped $NaGdF_4@NaYF_4$ ($Pr^{3+}$ = 0.1 mol. %, $Yb^{3+}$ = 6 mol. %) samples. (c) Comparison of NIR luminescence spectra for the $Pr^{3+}/Yb^{3+}$ codoped $NaGdF_4@Yb^{3+}$:$NaYF_4$ ($Pr^{3+}$ = 0.1 mol. %, $Yb^{3+}$ = 4 mol. %) and $Pr^{3+}/Yb^{3+}$ codoped $NaGdF_4@NaYF_4$ NPs ($Pr^{3+}$ = 0.1 mol. %, $Yb^{3+}$ = 10 mol. %) samples. (d) Luminescence spectra for the $Pr^{3+}/Yb^{3+}$ codoped $NaGdF_4@$ $Yb^{3+}$:$NaYF_4$ ($Pr^{3+}$ = 0.1 mol. %, $Yb^{3+}$ = 4 mol. %) samples. Reproduced with permission from Zhu *et al.*, Nanoscale **6**, 10500 (2014). Copyright The Royal Society of Chemistry (RSC), see http://pubs.rsc.org/en/content/articlelanding/2014/nr/c4nr02785j#!divAbstract.

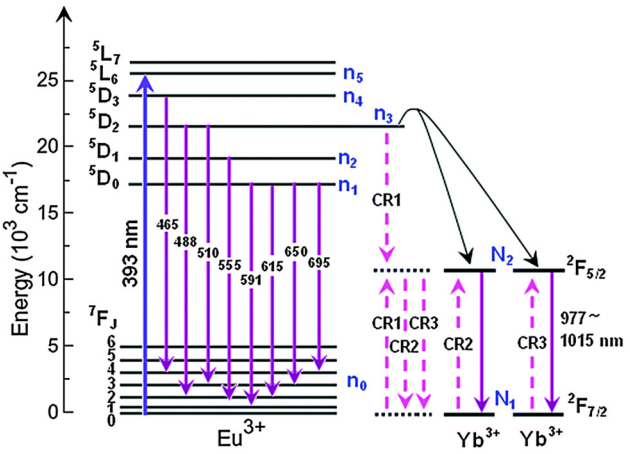


FIG. 11. Energy-level diagram of the $Eu^{3+}/Yb^{3+}$ system shows the ET mechanism of IR quantum cutting from $^5D_2$ ($Eu^{3+}$) to $^2F_{7/2}$ ($Yb^{3+}$). A 393 nm excitation source was used. Reproduced with permission from Wang *et al.*, Phys. Chem. Chem. Phys. **16**, 13440 (2014). Copyright The Royal Society of Chemistry (RSC), see http://pubs.rsc.org/en/content/articlelanding/2014/cp/c4cp01263a#!divAbstract.

imaging, etc. The NIR light can easily penetrate through the biological tissues and can be tuned to destroy infectious diseases in the body. Since the RE doped fluoride nanophosphors are excited by NIR (976 nm) light, the damage of tissue through the use of high energy visible even near UV photon can be avoided. The RE doped

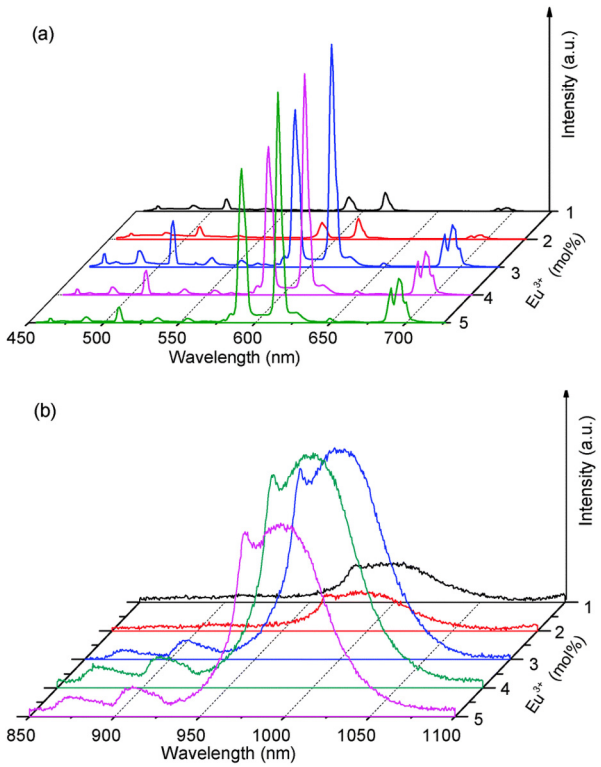


FIG. 12. Emission spectra of $Eu^{3+}$ at different concentrations: (a) visible and (b) IR luminescence. A 393 nm excitation source was used to illuminate the sample. Reproduced with permission from Wang *et al.*, Phys. Chem. Chem. Phys. **16**, 13440 (2014). Copyright The Royal Society of Chemistry (RSC), see http://pubs.rsc.org/en/content/articlelanding/2014/cp/c4cp01263a#!divAbstract.

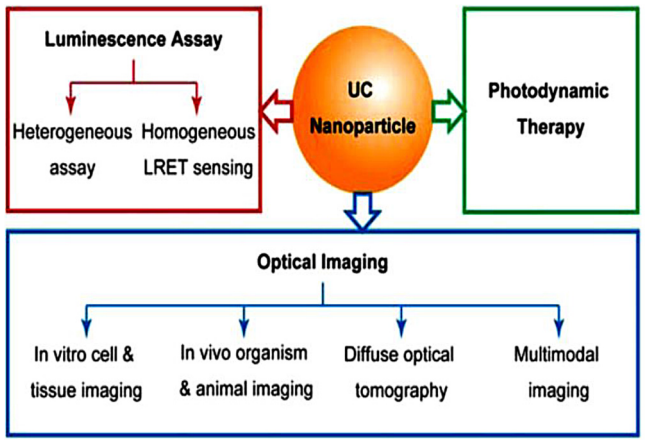


FIG. 13. Schematic diagram showing the application of RE doped UCNPs. Reproduced with permission from Wang *et al.*, Analyst **135**, 1839 (2010). Copyright The Royal Society of Chemistry (RSC), see http://dx.doi.org/10.1039/C0AN00144A.

fluoride nanophosphors are nontoxic and more stable and thus a state of art with potential applications in biological and clinical laboratories.[68–87] The use of RE doped materials in different fields can be understood with the following schematic diagram (Fig. 13).[96]

The RE doped fluoride nanophosphors show color tunability[97–99] and temperature sensing ability.[99,100] Zhang *et al.* have studied the color tuning nature of UC emission intensity from green to red in $NaScF_4$ doped with $Yb^{3+}/Er^{3+}$ nanocrystals by controlling the time of reaction.[97] They observed that the shorter the reaction time, the larger the number of crystal defects which would lead to the color tuning from green to red due to an increase in the nonradiative transitions and thus have potential uses in photonics. The RE ions have thermocoupled energy levels and a slight change in the temperature can tune the population of the ions

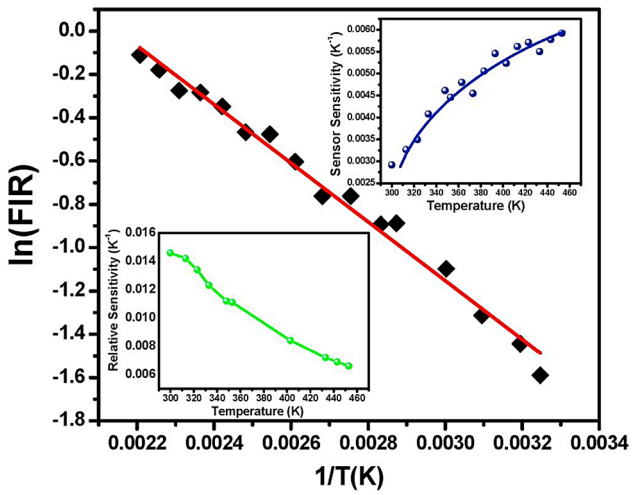


FIG. 14. Graph showing the relationship between ln(FIR) and inverse absolute temperature. Insets show the sensor sensitivity and relative sensitivity corresponding to upper and lower windows, respectively. Reprinted with permission from Dubey *et al.*, J. Alloys Compd. **693**, 194–200. Copyright 2017 Elsevier.

in these levels. This change can be monitored by observation of the emission spectra of the RE ions at different temperatures starting at room temperature.[100,101] It can be used in nanothermometry to show small variations in the temperature of human bodies at an intracellular scale.[100] For example, Dubey *et al.*[100] have studied the optical nanothermometry in the $NaYF_4$:$Er^{3+}$/$Yb^{3+}$/$Li^+$ phosphors and found an enhancement in the temperature sensing in the presence of $Li^+$ ions with a maximum sensor sensitivity of ~0.0059 $K^{-1}$. Figure 14 shows the sensor sensitivity (upper inset) and relative sensitivity (lower inset) of the $Er^{3+}$/$Yb^{3+}$/$Li^+$ triply ions doped $NaYF_4$ phosphor for the $^2H_{11/2} \rightarrow {}^4I_{15/2}$ and $^4S_{3/2} \rightarrow {}^4I_{15/2}$ transitions of the $Er^{3+}$ ions at different temperatures.

The RE doped fluoride nanophosphors have numerous applications in the field of biological related activities. The RE doped fluoride nanophosphors have intense narrow band sharp emission lines free from photobleaching, autofluorescence, and have a long lifetime. They can overcome the shortcomings of the molecular dyes currently used. Hu *et al.* have studied upconverting RE mPEG-UCNPs (i.e., $LaF_3$:20% Yb, 1% Ho) nanophosphors as biological labels.[102] Basically, the cell-cytotoxicity and cell-permeability of luminescent materials are very important parameters to check for their compatibility for use of such materials as bioprobes. The cytotoxicity analysis shows that the mPEG-UCNPs are less toxic with a cell viability up to 80% for an increase in the concentration from 125 to 250 $\mu g\,ml^{-1}$. The fluorescence and bright-field laser scanning confocal microscope images show the fluorescence through the intracellular region with negligible background fluorescence (Fig. 15).

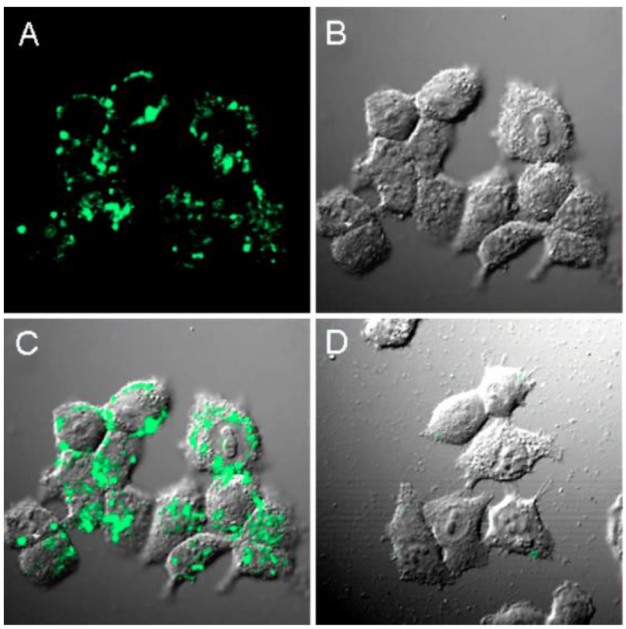


FIG. 15. Human nasopharyngeal epidermal carcinoma cell line (KB cells) were captured with confocal luminescence and bright-field images. (a) Confocal luminescence images of cells (100 $\mu g\,ml^{-1}$ mPEG-UCNPs was stained @ 2 h at 37 °C), excitation of 980 nm was used. (b) Bright-field image [panel (a)]. (c) The image captured after superimposing [(a) and (b)]. (d) Images of confocal luminescence and bright-field after superimposing both 100 $\mu g\,ml^{-1}$ mPEG-UCNPs (green) was stained @ 2 h at 4 °C. Reprinted with permission from Hu *et al.*, Chem. Mater. **20**, 7003 (2008). Copyright 2008 American Chemical Society.

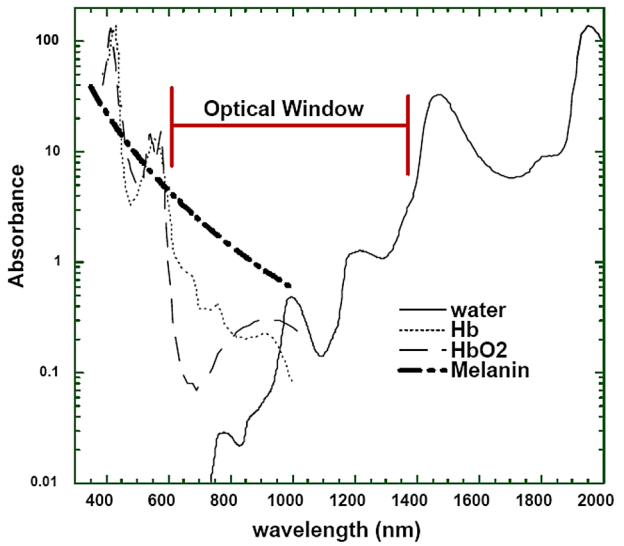


FIG. 16. Depiction of the optical window in human tissues due to the absorption of red and NIR wavelengths (600–1200 nm). Reprinted with permission from M. R. Hamblin and T. N. Demidova, Proc. SPIE **6140**, 614001 (2006). Copyright 2006 Society of Photo Optical Instrumentation Engineers.

For biological tissues of the human body, the absorption window of incident photons is from around 600 to 1400 nm. The absorption coefficients of water, melanin, deoxy-, and hemoglobin are very small in this regime (Fig. 16). The photons in this wavelength window penetrate more deeply into tissue than that of photons in the 400–750 nm wavelength range.[104] The IR photons are absorbed only in a small amount by the tissues and the rest of the incident photons are scattered. Therefore, a laser beam penetrates the tissue up to a few millimeters. The crucial applications of the tissue imaging are thus based on the specific optical window such as 860 nm, 1060 nm, and 1310 nm (based on the excitation wavelength of the material). But for the UC nanophosphor, the excitation wavelength is found to be 980 nm, which is a suitable wavelength for imaging purposes. This imaging technique is better than the whole body imaging techniques such as magnetic resonance imaging, X-rays, and ultrasound, because of the simple visual inspection at a fine spot, below <100 $\mu$m penetration depth. Moreover, this technique is also better due to its high resolution.

The RE doped UC fluoride nanophosphors are also used in fluorescence resonance energy transfer sensing of drug release and imaging based chemotherapy,[103] NIR imaging and photothermal treatment,[105] thermal scanning at the cellular level,[106] *in vivo* imaging, computed tomography (CT) and magnetic resonance (MR) imaging,[107,108] etc. For example, the trimodal properties of core-shell $BaYbF_5$:Tm@$BaGdF_5$:Yb,Tm nanophosphors have been investigated by Zhang *et al.* and applied these nanoparticles for *in vivo* trimodal upconversion luminescence/CT/MR imaging.[108] The core-shell $BaYbF_5$:Tm@$BaGdF_5$:Yb,Tm nanophosphors are nontoxic and appear clearly in *in vivo* UC

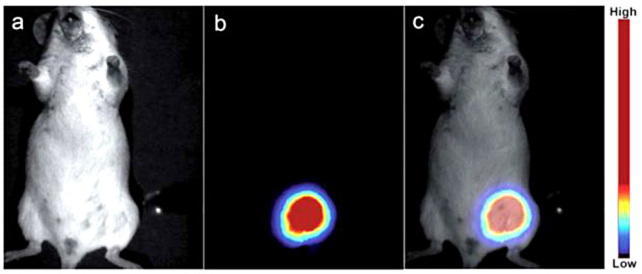


FIG. 17. $BaYbF_5$:Tm@$BaGdF_5$:Yb,Tm–PEG nanoparticles were injected in a mouse for *in vivo* UC luminescence imaging: (a) white-light imaging, (b) UC emission imaging, and (c) the overlay (superimposed) images of both (a) and (b). The excitation wavelength used for imaging was from 795 nm to 805 nm. Reproduced with permission from Zhang *et al.*, RSC Adv. **6**, 14283 (2016). Copyright The Royal Society of Chemistry (RSC), see http://pubs.rsc.org/en/content/articlelanding/2016/ra/c5ra22991j#!divAbstract.

fluorescence imaging of a mouse with injection of the nanocrystals (Fig. 17).

Moreover, the nanocrystals have the potential application in CT scanning. In the case of *in vivo* CT imaging, the images of Kunming mice were taken using iCT (Brilliance iCT, Philips Healthcare, Cleaveland, OH) many times before and after the injection of nanoparticles and iobitridol, respectively. A CT scan was taken before injection and after injection for 3 min, 30 min, 1 h, and 2 h. It has been observed after 3 min uptake of nanocrystals, the image quality of liver [Fig. 18(a)] and spleen [Fig. 18(b)] was enhanced up to 2 h. After 2 h, there was no enhancement observed. This phenomenon can easily be distinguished by using a volume rendering method [Fig. 18(c)].

The $Gd^{3+}$ ions show magnetic properties and are present in $BaYbF_5$:Tm@$BaGdF_5$:Yb/ Tm–PEG nanoparticles, which enable the enhancement of the $T_1$ MR imaging of mice. The MR signal has a similar effect in comparison to Gd–diethylene triamine pentacetate acid (DTPA) [Figs. 19(a) and 19(b)]. The Kunming mice have been scanned by using a 1.5 T clinical scanner to see *in vivo* $T_1$WI MR imaging. The muscle signal is shown in Figs. 19(c) and 19(d) without injection (arrow) and after the subcutaneous injection of nanoparticles with oval shape (arrow).

Furthermore, a review by Kumar *et al.*[109] demonstrates the preparation methods of the multifunctional $NaYF_4$ UC materials and recent trends for their multipurpose applications including light emitting diodes (LEDs) and solar cell devices. The conversion efficiency of photovoltaic (PV) cells

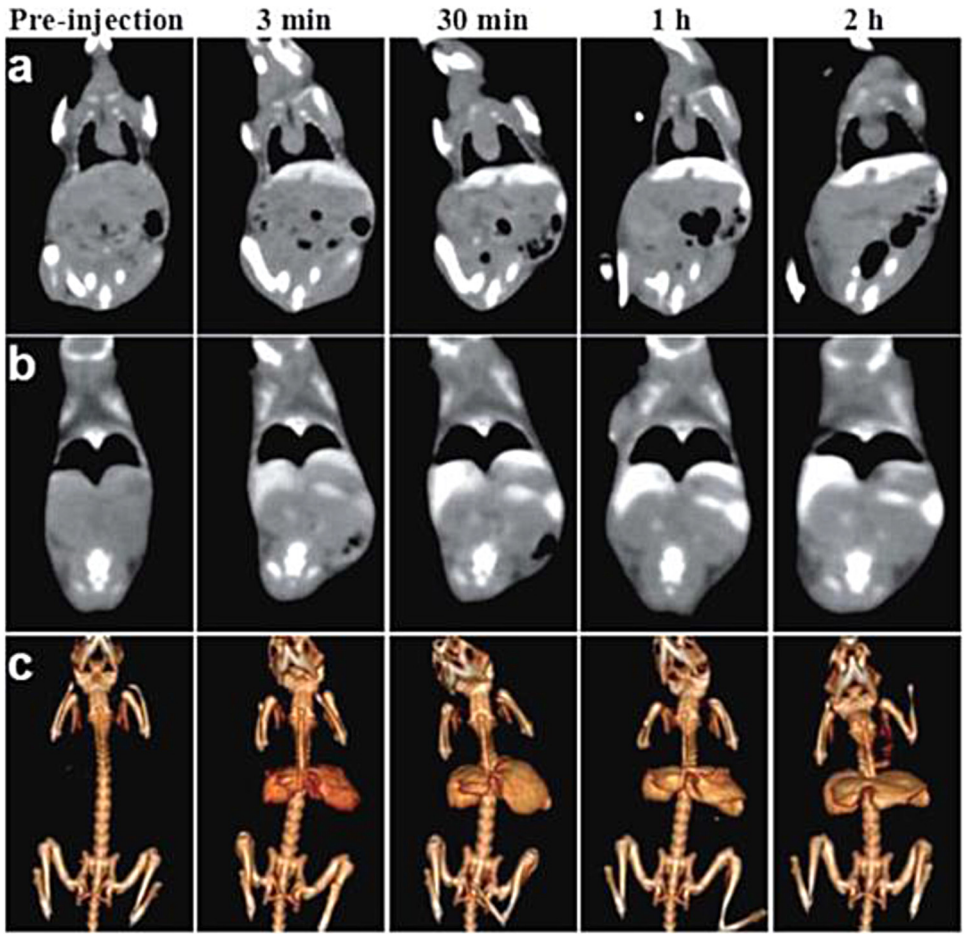


FIG. 18. CT scan images of mice (1 ml $BaYbF_5$:Tm@$BaGdF_5$:Yb/Tm–PEG nanoparticles was used to inject in 118 mM ml_1 solution). Different organs of mice such as the (a) liver, (b) spleen and kidney, and (c) volume rendering method of CT images are shown. Reproduced with permission from Zhang *et al.*, RSC Adv. **6**, 14283 (2016). Copyright The Royal Society of Chemistry (RSC), see http://pubs.rsc.org/en/content/articlelanding/2016/ra/c5ra22991j#!divAbstract.

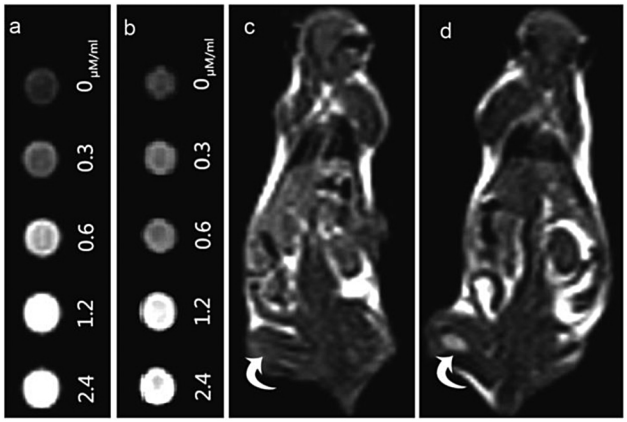


FIG. 19. (a) T1WI MR images of Gd–DTPA at different concentrations, (b) $BaYbF_5$:Tm@$BaGdF_5$:Yb/Tm–PEG nanoparticles are used for T1WI MR imaging at different concentrations, (c) the image of muscle signal before the injection of nanoparticles (arrow), and (d) the image of muscle signal after the injection of nanoparticles (arrow). Reproduced with permission from Zhang *et al.*, RSC Adv. **6**, 14283 (2016). Copyright The Royal Society of Chemistry (RSC), see http://pubs.rsc.org/en/content/articlelanding/2016/ra/c5ra22991j#!divAbstract.

is limited due to their insensitivity to the full solar spectrum. The spectral distribution of sunlight consists of photons with wavelengths that range from ultraviolet to infrared (280–2500 nm), Fig. 20. Current PV cells, however, only utilize a relatively small fraction of the solar photons.[110] The solar radiation spectrum shows the fraction (highlighted in green in the online version) absorbed by a typical crystalline silicon-based PV cell and the spectral regions that can be utilized through quantum cutting and UC processes (highlighted in purple and red, respectively, in the online version). The function of $NaYF_4$ nanophosphors to eliminate the spectral variance among the incident solar spectrum, semiconductor, and the sub-bandgap character of the semiconductor materials is argued explicitly. Some very good examples of $Er^{3+}$-doped/codoped $NaYF_4$ UC phosphors to enhance the responsivity in the NIR spectrum for solar cell applications are given in Table I.[109] The UC is especially relevant for amorphous Si solar cells.

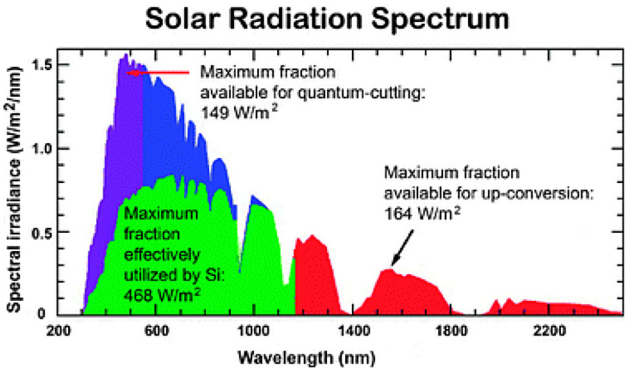


FIG. 20. Solar radiation spectrum showing the fraction (highlighted in green) absorbed by a typical crystalline silicon-based PV cell and the spectral regions that can be utilized through quantum-cutting and UC processes. Reprinted with permission from Richards, Solar Energy Mater. Solar Cells **90**, 2329–2337. Copyright 2006 Elsevier.

TABLE I. Selected lanthanide-doped $NaYF_4$ UC material used for solar cell applications. Reprinted with permission from Kumar *et al.*, Phys. B: Condens. Matter **535**, 278–286. Copyright 2018 Elsevier.

| Host lattice | Dopant ion | Excitation (nm) | Emission bands (nm) | Solar cell type | Reference |
|---|---|---|---|---|---|
| $aYF_4$ | $Er^{3+}$ | 1523 | 550, 660, 800, 980 | c-Si | 111 |
| $NaGdF_4$ | $Er^{3+}$ | 1530 | 527, 540, 653 | c-Si | 112 |
| $NaYF_4$ | $Yb^{3+}$, $Er^{3+}$ | 980, 1530 | 653, 520, 540 | a-Si | 113 |
| $NaYF_4$ | $Yb^{3+}$, $Er^{3+}$, $Gd^{3+}$ | 980 | 540, 660 | a-Si | 114 |
| $NaYF_4$ | $Er^{3+}$ | 1560, 980 | 522, 540, 650 | a-Si | 115 |
| $NaYF_4$ | $Yb^{3+}$, $Er^{3+}$ | 980 | 524, 540, 660 | dye-sensitized solar cell | 116 |
| $NaYF_4$ | $Yb^{3+}$, $Er^{3+}$ | 980 | 540, 660 | Organic | 117 |

The excitation wavelength of $NaYF_4$ phosphor with the right dopants also makes them suitable for phosphors in UV-pumped white LED devices.[118] The roles of the synthesized method and preparation conditions have severe effects on the efficiency thereof.[119] The UC properties can also be enhanced with codoping with transition metals.[120] Adusumalli *et al.*[121] used $NaYF_4$:$Ce^{3+}$/$Tm^{3+}$/$Mn^{2+}$ nanocrystals as an efficient single component phosphor in order to produce intense white light. The $Ce^{3+}$ ions were used as the excitation source, and the single blue band emission of $Tm^{3+}$ ions was combined with the broadband green–yellow emission of $Mn^{2+}$ ions to produce strong white-light emission.

## VI. SUMMARY AND CONCLUSIONS

This review summarizes the UC emission research in rare earth doped fluoride based phosphor materials. The SHG, TPE, and UC processes have been discussed and compared. The ESA as well as the basic energy transfer mechanisms involved in UC processes occurring in rare earth doped phosphors has also been discussed. The synthesis section includes synthesis methods, such as the coprecipitation method, hydrothermal method, and thermal decomposition method, which normally yield nanoscaled particles. The fluoride phosphors synthesized through these routes generally produce nanoparticles in the range of 10–50 nm. The nanoparticles in this range enable potential applications in fields such as solar cell, photonic devices, nanothermometry, biomarkers, and biological imaging. The NIR to visible UC process leads to applications of the rare earth doped fluoride phosphor materials in chemotherapy, photothermal treatment, theranostics, etc. It is found that these materials are also useful in medicinal and clinical laboratories for CT scan and MR imaging. Thus, the rare earth doped fluoride phosphors are very unique and promising materials for many functions and multidirectional applications. The scope of the use of these materials is endless.

## ACKNOWLEDGMENTS

The funding support is acknowledged to the South African Research Chairs Initiative of the Department of Science and Technology (DST) and the National Research Fund (NRF) (Grant No. 84415).

## CONFLICT OF INTEREST

There is no conflict of interest.

[1]S. K. Maurya, S. P. Tiwari, A. Kumar, and K. Kumar, J. Rare Earths **36**, 903 (2008).
[2]R. S. Yadav, R. K. Verma, and S. B. Rai, J. Phys. D: Appl. Phys. **46**, 275101 (2013).
[3]S. P. Tiwari, K. Kumar, and V. K. Rai, J. Appl. Phys. **118**, 183109 (2015).
[4]S. P. Tiwari, K. Kumar, and V. K. Rai, Appl. Phys. B: Laser Opt. **121**, 221 (2015).
[5]S. P. Tiwari, M. K. Mahata, K. Kumar, and V. K. Rai, Spectrochim. Acta A: Mol. Biomol. Spectrosc. **150**, 623 (2015).
[6]A. Kumar, M. H. Couto, S. P. Tiwari, K. Kumar, and J. C. Esteves da Silva, Chem. Select **3**, 10566 (2018).
[7]A. Kumar, S. P. Tiwari, K. Kumar, and A. K. Singh, Appl. Phys. B **122**, 190 (2016).
[8]R. S. Yadav, S. J. Dhoble, and S. B. Rai, New J. Chem. **42**, 7272 (2018).
[9]D. Yang, P. Ma, Z. Hou, Z. Cheng, C. Li, and J. Lin, Chem. Soc. Rev. **44**, 1416 (2015).
[10]J. Zhou, Z. Liu, and F. Li, Chem. Soc. Rev. **41**, 1323 (2012).
[11]J. Zhou, X. J. Zhu, M. Chen, Y. Sun, and F. Y. Li, Biomaterials **33**, 6201 (2012).
[12]Q. Chen, C. Wang, L. Cheng, W. He, Z. Cheng, and Z. Liu, Biomaterials **35**, 2915 (2014).
[13]D. H. Kim and J. U. Kang, Microsc. Sci. Technol. Appl. Educ. 571 (2010).
[14]T. Kano, H. Yamamoto, and Y. Otomo, J. Electrochem. Soc. **119**, 1561 (1972).
[15]A. Pandey, V. K. Rai, V. Kumar, V. Kumar, and H. C. Swart, Sen. Act. B: Chem. **209**, 352 (2015).
[16]R. E. Thoma, H. Insley, and G. M. Hebert, Inorg. Chem. **5**, 1222 (1966).
[17]J. H. Burns, Inorg. Chem. **4**, 88 (1965).
[18]H. S. Kiliaan, J. F. Kotte, and G. Lasse, Chem. Phys. Lett. **133**, 425 (1987).
[19]D. Zakaria, R. Mahiou, D. Avignant, and M. Zahir, J. Alloys Compd. **257**, 65 (1997).
[20]N. Bloembergen, "Solid state infrared quantum counters," Phys. Rev. Lett. **2**, 84 (1959).
[21]A. Pandey, S. P. Tiwari, V. Dutta, and V. Kumar, IGI Global **86** (2018).
[22]F. Auzel, "UC and anti-Stokes processes with f and d ions in solids," Chem. Rev. **104**, 139 (2004).
[23]B. R. Masters and P. T. C. So, *Handbook of Biomedical Nonlinear Optical Microscopy* (Oxford University, Oxford, 2008).
[24]P. N. Prasad, *Introduction to Biophotonics* (John, Wiley & Sons, Inc., Hoboken, NJ, 2003).
[25]M. F. Joubert, Opt. Mater. **11**, 181 (1999).
[26]S. P. Tiwari, A. Kumar, and K. Kumar, Res. Front. Sci. 23 (2016).
[27]G. Y. Chen, Y. Liu, Y. G. Zhang, G. Somesfalean, Z. G. Zhang, Q. Sun, and F. P. Wang, Appl. Phys. Lett. **91**, 133103 (2007).
[28]G. Y. Chen, Y. G. Zhang, G. Somesfalean, Z. G. Zhang, Q. Sun, and F. P. Wang, Appl. Phys. Lett. **89**, 163105 (2006).
[29]G. Y. Chen, G. Somesfalean, Z. G. Zhang, Q. Sun, and E. P. Wang, Opt. Lett. **32**, 87 (2007).
[30]G. Chen, Q. Hailong, P. N. Prasad, and X. Chen, Chem. Rev. **114**, 5161 (2014).
[31]G. Y. Chen, T. Y. Ohulchanskyy, R. Kumar, H. Agren, and P. N. Prasad, ACS Nano **4**, 3163 (2010).
[32]Y. J. Sun, Y. Chen, L. J. Tian, Y. Yu, X. G. Kong, J. W. Zhao, and H. Zhang, Nanotechnology **18**, 275609 (2007).
[33]L. Y. Wang and Y. D. Li, Chem. Commun. **28**, 2557 (2006).
[34]K. W. Kramer, D. Biner, G. Frei, H. U. Gudel, M. P. Hehlen, and S. R. Luthi, Chem. Mater. **16**, 1244 (2004).
[35]Y. Dwivedi, S. N. Thakur, and S. B. Rai, Appl. Phys. B: Laser Opt. **89**, 45 (2007).
[36]H. J. Liang, G. Y. Chen, L. Li, Y. Liu, F. Qin, and Z. G. Zhang, Opt. Commun. **282**, 3028 (2009).
[37]A. A. Pushkar, T. V. Uvarova, and V. V. Kiiko, Opt. Spectrosc. **111**, 273 (2011).
[38]G. Ledoux, M. F. Joubert, and S. Mishra, *Photonic & Electronic Properties of Fluoride Materials*, edited by A. Tressaud and K. R. Poeppelmeir (Elsevier, France, 2016), pp. 35–64.
[39]G. M. Pound and V. K. L. Mer, J. Am. Chem. Soc. **74**, 2323 (1952).
[40]V. K. Lamer and R. H. Dinegar, J. Am. Chem. Soc. **72**, 4847 (1950).
[41]X. Liu, X. Zhang, G. Tian, W. Yin, L. Yan, L. Ruan, Z. Yang, D. Xiao, and Z. Gu, Cryst. Eng. Comm. **16**, 5650 (2014).
[42]F. Vetrone, V. Mahalingam, and J. A, Capobianco Chem. Mater. **21**, 1847 (2009).
[43]R. H. Page, K. I. Schaffers, P. A. Waide, J. B. Tassano, S. A. Payne, W. F. Krupke, and W. K. Bischel, J. Opt. Soc. Am. B **15**, 996 (1998).
[44]G. S. Yi, H. C. Lu, S. Y. Zhao, G. Yue, W. J. Yang, D. P. Chen, and L.-G. Guo, Nano Lett. **4**, 2191 (2004).
[45]M. Wang, G. Abbineni, A. Clevenger, C. Mao, and S. Xu, Nanomed. Nanotechnol. Biol. Med. **7**, 710 (2011).
[46]C. Li, J. Yang, Z. Quan, P. Yang, D. Kong, and J. Lin, Chem. Mater. **19**, 4933 (2007).
[47]C. Li, Z. Quan, J. Yang, P. Yang, and J. Lin, Inorg. Chem. **46**, 6329 (2007).
[48]J. Ladol, H. Khajuria, S. Khajuria, and H. N. Sheikh, Bull. Mater. Sci. **39**, 943 (2016).
[49]Y. Shang, H. Shuwei, L. Jing, T. Meiling, W. Ning, C. Yang, and G. Chen, Nanomaterials **5**, 218 (2015).
[50]A. Kumar, S. P. Tiwari, A. Sardar, K. Kumar, and J. E. da Silva, Sens. Actuat. A Phys. **280**, 179 (2018).
[51]Y. Liu, D. Tu, H. Zhu, and X. Chen, Chem. Soc. Rev. **42**, 6924 (2013).
[52]J. C. Boyer, F. Vetrone, L. A. Cuccia, and J. A. Capobianco, J. Am. Chem. Soc. **128**, 7444 (2006).
[53]J. C. Boyer, L. A. Cuccia, and J. A. Capobianco, Nano Lett. **7**, 847 (2007).
[54]F. Vetrone, R. Naccache, V. Mahalingam, C. G. Morgan, and J. A. Capobianco, Adv. Funct. Mater. **19**, 2924 (2009).
[55]R. Naccache, F. Vetrone, V. Mahalingam, L. A. Cuccia, and J. A. Capobianco, Chem. Mater. **21**, 717 (2009).
[56]Q. Liu, Y. Sun, T. Yang, W. Feng, C. Li, and F. Li, J. Am. Chem. Soc. **133**, 17122 (2011).
[57]H. T. Wong, F. Vetrone, R. Naccache, H. L. W. Chan, J. Hao, and J. A. Capobianco, J. Mater. Chem. **21**, 16589 (2011).
[58]A. Kumar, S. P. Tiwari, K. Kumar, and J. C. E. da Silva, J. Alloys Compd. **776**, 207 (2019).
[59]Z. Quan, D. Yang, P. Yang, X. Zhang, H. Lian, X. Liu, and J. Lin, Inorg. Chem. **47**, 9509 (2008).
[60]M. Haase and H. Schafer, Angew. Chem. Int. Ed. **50**, 5808 (2011).
[61]F. Zhang, "Upconversion luminescence of lanthanide ion-doped nanocrystals," in *Photon Upconversion Nanomaterials* (Springer, Berlin, Heidelberg, 2015), pp. 73–119.
[62]H. Q. Wang and T. Nann, in *Lanthanide Luminescence*, edited by P. Hanninen and H. Harma (Springer, Berlin, 2011), pp. 115–132.
[63]F. Wang and X. Liu, Chem. Soc. Rev. **38**, 976 (2009).
[64]H. X. Mai, Y. W. Zhang, L. D. Sun, and C. H. Yan, J. Phys. Chem. C **111**, 13730 (2007).
[65]P. Yuan, Y. H. Lee, M. K. Gnanasammandhan, Z. Guan, Y. Zhang, and Q. H. Xu, Nanoscale **4**, 5132 (2012).
[66]H. X. Mai, Y. W. Zhang, R. Si, Z. G. Yan, L. Sun, L. P. You, and C. H. Yan, J. Am. Chem. Soc. **19**, 6426 (2006).
[67]M. Lin, Y. Zhao, S. Wang, M. Liu, Z. Duan, Y. Chen, F. Li, F. Xu, and T. Lu, Biotech. Adv. **30**, 1551 (2012).
[68]R. Weissleder and M. J. Pittet, Nature **452**, 580 (2008).
[69]J. Cheon and J. H. Lee, Acc. Chem. Res. **41**, 1630 (2008).
[70]J. Xie, G. Liu, H. S. Eden, H. B. Ai, and X. Y. Chen, Acc. Chem. Res. **44**, 883 (2011).
[71]H. Kobayashi, M. Ogawa, R. Alford, P. L. Choyke, and Y. Urano, Chem. Rev. **110**, 2620 (2010).
[72]D. R. Larson, W. R. Zipfel, R. M. Williams, S. W. Clark, M. P. Bruchez, F. W. Wise, and W. W. Webb, Science **300**, 1434 (2003).
[73]L. A. Bentolila, Y. Ebenstein, and S. Weiss, J. Nucl. Med. **50**, 493 (2009).

[74]B. N. G. Giepmans, S. R. Adams, M. H. Ellisman, and R. Y. Tsien, Science **312**, 217 (2006).
[75]T. Terai and T. Nagano, Curr. Opin. Chem. Biol. **12**, 515 (2008).
[76]M. Beija, C. A. M. Afonso, and J. M. G. Martinho, Chem. Soc. Rev. **38**, 2433 (2009).
[77]M. Zhang *et al.*, J. Am. Chem. Soc. **129**, 10322 (2007).
[78]Q. Zhao, F. Y. Li, and C. H. Huang, Chem. Soc. Rev. **39**, 3007 (2010).
[79]Q. Zhao, C. H. Huang, and F. Y. Li, Chem. Soc. Rev. **40**, 2508 (2011).
[80]K. K. W. Lo, S. P. Y. Li, and K. Y. Zhang, New J. Chem. **35**, 265 (2011).
[81]S. V. Eliseeva and J. C. G. Bunzli, Chem. Soc. Rev. **39**, 189 (2010).
[82]X. Michalet *et al.*, Science **307**, 538 (2005).
[83]F. Wang, W. B. Tan, Y. Zhang, X. P. Fan, and M. Q. Wang, Nanotechnology **17**, 1 (2006).
[84]W. M. Yen and M. J. Weber, *Inorganic Phosphors: Compositions, Preparation and Optical Properties* (CRC, FL, 2004).
[85]G. Blasse and B. C. Grabmaier, *Luminescent Materials* (Springer, Berlin, 1994).
[86]K. Riwotzki, H. Meyssamy, H. Schnablegger, A. Kornowski, and M. Haase, Angew. Chem. Int. Ed. **40**, 573 (2001).
[87]Q. Dou, L. Jiang, D. Kai, C. Owh, and X. J. Loh, Drug Discov. Today **22**, 1400 (2017).
[88]L. Guo, Y. Wang, J. Zhang, Y. Wang, and P. Dong, Nano Res. Lett. **7**, 636 (2012).
[89]J. Zhang, Y. Wang, L. Guo, and P. Dong, Dalton Trans. **42**, 3542 (2013).
[90]S. Zaske, L. Andreas, and B. Christoph, Opt. Exp. **19**, 12825 (2011).
[91]D. C. Yu, X. Y. Huang, S. Ye, and Q. Y. Zhang, J. Alloys Compd. **509**, 9919 (2011).
[92]F. Wang and X. G. Liu, J. Am. Chem. Soc. **130**, 5642 (2008).
[93]D. C. Yu, S. Ye, M. Y. Peng, Q. Y. Zhang, and L. Wondraczek, Appl. Phys. Lett. **100**, 191911 (2012).
[94]W. Zhu, D. Chen, L. Lei, J. Xu, and Y. Wang, Nanoscale **6**, 10500 (2014).
[95]X. Wang, C. Liu, T. Yu, and X. Yan, Phys. Chem. Chem. Phys. **16**, 13440 (2014).
[96]F. Wang, D. Banerjee, Y. Liu, X. Chen, and X. Liu, Analyst **135**, 1839 (2010).
[97]L. Zhang, S. Zhao, Z. Liang, J. Zhang, W. Zhu, P. Liu, and H. Sun, J. Alloys Compd. **699**, 1 (2017).
[98]Z. Li, L. Wang, Z. Wang, X. Liu, and Y. Xiong, J. Phys. Chem. C **115**, 3291 (2011).
[99]S. Heer, O. Lehmann, M. Hasse, and H.-U. Güdel, Angew. Chem., Int. Ed. **42**, 3179 (2003).
[100]A. Dubey, A. K. Soni, A. Kumari, R. Dey, and V. K. Rai, J. Alloys Compd. **693**, 194 (2017).
[101]D. Li, Q. Shao, Y. Dong, and J. Jiang, J. Alloys Compd. **617**, 1 (2014).
[102]H. Hu, M. X. Yu, F. Y. Li, Z. G. Chen, X. Gao, L. Q. Xiong, and C. Huang, Chem. Mater. **20**, 7003 (2008).
[103]J. Xu *et al.*, Chem. Mater. **29**, 7615 (2017).
[104]M. R. Hamblin and T. N. Demidova, Proc. SPIE **6140**, 614001 (2006).
[105]G. Shan, R. Weissleder, and S. A. Hilderbrand, Theranostics **3**, 267 (2013).
[106]P. R. Sevilla, Y. Zhang, P. H. Gonzalez, F. S. Rodriguez, F. J. Sole, X. Liu, and D. Jaque, Adv. Mater. **28**, 2421 (2016).
[107]J. Zhou, Y. Sun, X. Du, L. Xiong, H. Hu, and F. Li, Biomaterials **31**, 3287 (2010).
[108]P. Zhang, Y. He, J. Liu, J. Feng, Z. Sun, P. Lei, Q. Yuan, and H. Zhang, RSC Adv. **6**, 14283 (2016).
[109]D. Kumar, S. Verma, K. Verma, S. Som, V. Sharma, V. Kumar, and H. C. Swart, Phys. B: Condens. Matter **535**, 278 (2018).
[110]B. S. Richards, Sol. Energy Mater. Sol. Cells **90**, 2329 (2006).
[111]A. Shalav, B. S. Richards, T. Trupke, K. W. Krämer, and H. U. Güdel, Appl. Phys. Lett. **86**, 013505 (2005).
[112]F. Xin, S. Zhao, L. Huang, D. Deng, G. Jia, H. Wang, and S. Xu, Mater. Lett. **78**, 75 (2012).
[113]X. D. Zhang, X. Jin, D. F. Wang, S. Z. Xiong, X. H. Geng, and Y. Zhao, Phys. Status Solidi c **7**, 1128 (2010).
[114]Z. Q. Li, X. D. Li, Q. Q. Liu, X. H. Chen, Z. Sun, C. Liu, and S. M. Huang, Nanotechnology **23**, 025402 (2011)
[115]Y. Chen, W. He, Y. Jiao, H. Wang, X. Hao, J. Lu, and S. E. Yang, J. Lumin. **132**, 2247 (2012).
[116]J. Chang, Y. Ning, S. Wu, W. Niu, and S. Zhang, Adv. Funct. Mater. **23**, 5910 (2013).
[117]J. L. Wu, F. C. Chen, S. H. Chang, K. S. Tan, and H. Y. Tuan, Org. Elect. **13**, 2104 (2012).
[118]T. K. Pathak, A. Kumar, H. C. Swart, and R. E. Kroon, Phys. B: Condens. Matter **535**, 132 (2018).
[119]E. Palo *et al.*, Opt. Mater. **59**, 49 (2016).
[120]M. Tuomisto, E. Palo, T. Laihinen, I. Hyppanen, M. Lastusaari, H. C. Swart, and J. Holsa, Opt. Mater. **59**, 115 (2016).
[121]V. N. K. B. Adusumalli, H. V. S. R. M. Koppisetti, and V. Mahalingam, Chem. A Eur. J. **23**, 18134 (2017).